Nonlocal Response and Anamorphosis: The Case of Few-Layer Black Phosphorus

A. Mishchenko,[*,†] Y. Cao,[†,‡] G. L. Yu,[†] C. R. Woods,[†] R. V. Gorbachev,[†,‡] K. S. Novoselov,[†] A. K. Geim,[†,‡] and L. S. Levitov[*,§]

[†]School of Physics and Astronomy, University of Manchester, Manchester M13 9PL, United Kingdom
[‡]Centre for Mesoscience and Nanotechnology, University of Manchester, Manchester M13 9PL, United Kingdom
[§]Department of Physics, Massachusetts Institute of Technology, Cambridge, Massachusetts 02139, United States

S *Supporting Information*

ABSTRACT: Few-layer black phosphorus was recently rediscovered as a narrow-bandgap atomically thin semiconductor, attracting unprecedented attention due to its interesting properties. One feature of this material that sets it apart from other atomically thin crystals is its structural in-plane anisotropy which manifests in strongly anisotropic transport characteristics. However, traditional angle-resolved conductance measurements present a challenge for nanoscale systems, calling for new approaches in precision studies of transport anisotropy. Here, we show that the nonlocal response, being exponentially sensitive to the anisotropy value, provides a powerful tool for determining the anisotropy in black phosphorus. This is established by combining measurements of the orientation-dependent nonlocal resistance response with the analysis based on the *anamorphosis* relations. We demonstrate that the nonlocal response can differ by orders of magnitude for different crystallographic directions even when the anisotropy is at most order-one, allowing us to extract accurate anisotropy values.

KEYWORDS: *black phosphorus, phosphorene, nonlocal transport, conductance anisotropy, anamorphosis*
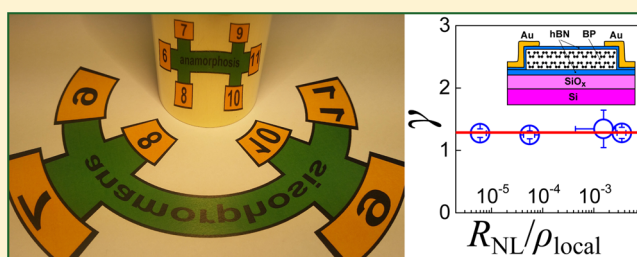
Black phosphorus (BP), a layered crystal allotrope of phosphorus, is composed of corrugated sheets of phosphorene held together by weak van der Waals interactions.[1] In phosphorene sheets, each phosphorus atom covalently bonds to its three nearest neighbors, forming warped hexagons in a nonplanar, chair conformation. This sp[3]-type bonding results in a distinctly anisotropic crystal structure: phosphorene adopts an accordion-like folded hexagonal lattice with grooves running along the y axis (with zigzag termination). Such crystal structure leads to highly anisotropic energy bands:[2] electrons and holes of phosphorene are nearly an order of magnitude heavier in the y direction (zigzag) as compared to the x direction (armchair). This results in an interesting in-plane anisotropy in electronic, optical, and acoustic properties.[3] Further, electrical conductivity and carrier mobility are higher along the x axis than along the y axis, whereas the opposite anisotropy sign is predicted for thermal conductance, a property that can potentially lead to high-efficiency thermoelectric devices.[4] The in-plane anisotropy is also of interest for plasmonics because the plasmon resonance frequency could be tuned with the light polarization due to the highly anisotropic nature of plasmons in BP.[5] However, although being of high interest because of their promise for device research and engineering, the anisotropic properties are currently lacking reliable characterization techniques. Here, we develop a new

approach that is particularly well suited for nanosystems where other known techniques can perform poorly or lack precision.

Transport anisotropy was studied recently in a two-terminal configuration by angle-resolved conductance measurements.[6,7] Refs 6 and 7 employed a circular geometry, measuring two-terminal conductance between sets of opposite contacts spaced by 30° or 45°. The angular dependence for the two-terminal conductance was fitted to an expression $\sigma(\theta) = \sigma_{xx}\cos^2\theta + \sigma_{yy}\sin^2\theta$, with θ the angle between the chosen pair of opposite contacts and the x axis. From the measured dependence, both the crystallographic orientation and the values σ_{xx} and σ_{yy} could be inferred, giving the anisotropy value

$$A = \sigma_{xx}/\sigma_{yy} \qquad (1)$$

ranging from 1.5 to 1.8. Unfortunately, such direct two-terminal measurements are prone to inaccuracy due to contact resistance and variability in device geometry, and thus are expected to yield relatively large errors in the inferred anisotropy values.

Here, we employ a different approach. We obtain the in-plane anisotropy from nonlocal measurements in a four-terminal geometry, in which a pair of current leads is positioned

far from the pair of voltage probes. Our rationale for resorting to such a method is the exponential sensitivity of the nonlocal signal to the anisotropy value. The exponential character of the nonlocal response follows from the seminal van der Pauw theorem,[8] which stipulates a relation between four-terminal resistance values $R_{ij,kl} = V_{ij}/I_{kl}$ obtained for the contacts k,l and i,j used as current leads and voltage probes, respectively. This theorem connects the nonlocal resistance values for different combinations of voltage and current contacts in arbitrary-shape homogeneous 2D samples. For an isotropic conductor of the sheet conductivity σ it reads $e^{-\pi\sigma R_{12,34}} + e^{-\pi\sigma R_{23,41}} = 1$, where the values $R_{ij,kl}$ depend on contact placement. Applied to long samples of dimensions $L \times W$, $L/W \gg 1$ with two pairs of contacts placed at opposite ends, the van der Pauw relations predict an exponential dependence of the nonlocal response on the aspect ratio

$$R_{\mathrm{nl}} \propto \rho e^{-\pi L/W}, \qquad \rho = \sigma^{-1} \tag{2}$$

Below, we extend this relation to anisotropic media using the *anamorphosis* (reshaping) theorem.[9]

The anamorphosis theorem stipulates that the multiterminal resistance values $R_{ij,kl}$ *remain unchanged* upon reshaping the sample via an anisotropic rescaling of the coordinates along the principal conductivity axes[10−14]

$$x = \gamma^{1/2}x', \qquad y = \gamma^{-1/2}y', \qquad \gamma = (\sigma_{xx}/\sigma_{yy})^{1/2} \tag{3}$$

and simultaneously letting the conductivity of the reshaped system to be isotropic and equal

$$\sigma' = (\sigma_{xx}\sigma_{yy})^{1/2} \tag{4}$$

For long samples with the major axis parallel to the x or y axis, the reshaping gives $L/W = \gamma^{\pm 1}L'/W' \gg 1$, respectively. The van der Pauw relation then predicts an exponential nonlocal response altered by the anisotropy as

$$R_{\mathrm{nl}}^{(x)} \propto \rho'\exp\left(-\frac{\pi L}{W\gamma}\right), \qquad R_{\mathrm{nl}}^{(y)} \propto \rho'\exp\left(-\frac{\pi L\gamma}{W}\right) \tag{5}$$

where we defined $\rho' = 1/\sigma'$. Here $R_{\mathrm{nl}}^{(x)}$ and $R_{\mathrm{nl}}^{(y)}$ denote the nonlocal response for long samples aligned with the x or y axis, respectively. Our argument based on reshaping indicates robustness of the exponential γ dependence. The order-one prefactors in eq 5, which in general are not universal, will be analyzed below for a strip geometry.

The strong dependence on γ suggests that nonlocal measurements afford a precision tool for determining the anisotropy. To exploit this opportunity, we fabricated multiterminal Hall bars aligned with the x and y crystallographic axes of black phosphorus, see Figure 1a−c. As discussed below, conductance anisotropy can then be extracted from the ratio of the nonlocal and local resistance. We found this approach to be reliable and robust despite a large variability in the nonlocal response values that could differ by orders of magnitude for different crystallographic directions.

To better understand the impact of anisotropy on the nonlocal response, eq 5, we first consider an *isotropic* conductor shaped into a Hall bar as in Figure 1b. When current is passed between, for example, contacts 2 and 3, it mostly flows straight across the device, with an exponentially small fraction flowing sideways, as the continuity equation requires that current does not drop to zero abruptly in the device channel. This produces stray currents which give rise to a voltage drop across remote
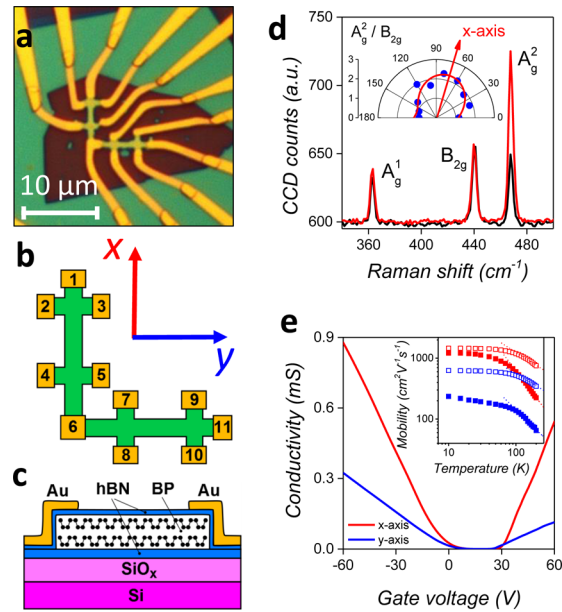

Figure 1. Fabrication and characterization of crystal-axes-aligned devices of hBN-encapsulated few-layer phosphorene. (a), (b) Device micrograph and schematics: two orthogonal Hall bars oriented along the x (easy) and y (hard) crystal axes. (c) Device cross-section: BP, encapsulated with hBN on SiO$_x$/Si substrate, connected to gold contacts through tunnel barriers provided by the monolayer hBN. (d) Polarization-dependent Raman spectra measured along two principal axes of hBN-encapsulated BP (x axis, red; y axis, black). Inset: Angle-resolved Raman signature A_g^2/B_{2g} used to determine the crystallographic orientation of a BP flake. (e) Four-terminal conductivity of hBN-encapsulated BP vs gate voltage measured at $T = 5$ K and bias voltage of 0.1 V (x axis, red; y axis, blue). Inset: temperature dependence of the field-effect mobility for electrons (solid squares) and holes (empty squares).

contacts 4 and 5 (Figure 1b). Analysis predicts a nonlocal resistance that decays exponentially with the separation L between current leads and voltage probes[15]

$$R_{\mathrm{nl}} \equiv \frac{V_{4,5}}{I_{2,3}} = \frac{2\rho}{\pi}\ln\coth\left(\frac{\pi L}{2W}\right) \approx \frac{4}{\pi}\rho\exp\left(-\frac{\pi L}{W}\right) \tag{6}$$

where the asymptotic exponential form gives accuracy better than 0.1% already for $L = W$.

A more complex behavior arises for an anisotropic conductor, where the anisotropic conductivity defines an easy (high-conductivity) and a hard (low-conductivity) direction for current flow. In this case, current applied along an easy direction is "pinched" into a relatively narrow path, which suppresses stray currents and reduces nonlocal response. In contrast, the current applied along a hard direction tends to spread out due to an "easy" transverse flow short-circuiting the direct "hard" flow. In this case, enhanced stray currents lead to a large nonlocal response. The resulting suppression and enhancement of R_{nl} in the two regimes is *exponential*, eq 5, with the corresponding exponents differing by the anisotropy factor $A = \gamma^2$.[9]

Next, we describe fabrication of the BP devices used in this work. Because few-layer black phosphorus is known to lack stability under ambient conditions,[16] we exfoliated BP crystals (purchased from HQ Graphene) in the inert atmosphere of a glovebox. In order to protect BP from oxygen and moisture, crystals were encapsulated with hexagonal boron nitride (hBN),

using the "dry peel" technique detailed elsewhere.[17,18] Starting with freshly exfoliated BP on a polymer film, a thin ($\approx$ 10 nm thickness) crystal was identified and picked up with a monolayer hBN on a polymer membrane.[19] The resulting stack was then transferred onto a 30−80 nm hBN which served as an atomically flat substrate. The dry transfer method ensures an extremely clean interface between BP and hBN crystals and protects the former from degradation when air-sensitive few-layer BP is exposed to ambient conditions for many months.[17] To avoid the degradation of BP surface during the fabrication procedures, the micromechanical exfoliation and transfer processes were performed in an argon environment provided by a glovebox with levels of H_2O and O_2 below 0.1 ppm. The final assembly on 290 nm SiO_x/p-Si wafer was taken out of the glovebox for subsequent microfabrication processing.

We used polarization-dependent Raman spectroscopy to establish the BP crystal axes orientation. Measurements were performed at room temperature in air using a confocal Witec spectrometer. Laser spot size of 0.5 μm was obtained by using a Nikon 100x objective. Samples were illuminated with green (2.41 eV) laser at 100 μW intensity. A high-density grating (1800 g/mm) was used to achieve energy resolution better than 2 cm^{-1}. Angular control of the sample, relative to the laser polarization, was made with a rotating stage giving an uncertainty of about $\pm$2 degrees. Black phosphorus features three main Raman modes:[20] A_g^1 for the z axis, out-of-plane phonons, A_g^2 for in-plane vibrations along the x axis (armchair), and B_{2g} for in-plane vibrations along the y axis (zigzag). The amplitude of the two in-plane modes is polarization-dependent with A_g^2 intensity maximal for laser polarization along the x axis (armchair), see Figure 1d. From the angular dependence of the normalized mode intensity A_g^2/B_{2g}, we extracted the crystallographic orientation of BP crystals, as shown in Figure 1d inset.

Subsequently, multiterminal Hall bar devices were defined via standard microfabrication techniques—e-beam lithography and metal deposition followed by reactive ion etching—with the device channel aligned with the x or y axis, Figure 1a−c. Because the encapsulating hBN monolayer has relatively low (<1 kΩ·μm^2) tunnel resistivity,[21] the electrodes (5 nm Cr adhesion layer followed by 100 nm Au) were deposited directly onto it, Figure 1c. Two devices (A and B) were studied in this work, each device comprising two orthogonal Hall bars defined along the x and y crystallographic axes. Devices A and B had channel length-to-width ratio L/W of 3 and 2.5, respectively, with W = 1 μm for both devices. Here we define the length L as the distance between voltage probes (e.g., 2 and 4 or 8 and 10 in Figure 1b), the same length scale will be relevant for nonlocal measurements; see below. To characterize transport properties, we measured four-terminal conductivity along both the x and y axes. DC conductivity was obtained by passing current through contact 1 to contact 11 and measuring voltage drop across, for example, contacts 2 and 4 for σ_{xx} and contacts 8 and 10 for σ_{yy}, see Figure 1b. Conductivity values were calculated as $\sigma_{xx} = R_{xx}^{-1}L/W$, $\sigma_{yy} = R_{yy}^{-1}L/W$.

Our field-effect transistor devices showed ambipolar behavior with somewhat enhanced hole-type transport (a likely result of p-type doping during crystal growth), as illustrated in Figure 1e for device B. The overall device performance was comparable with that reported previously.[22] We extracted field-effect mobilities μ_{xx}, μ_{yy} from the slopes $\delta\sigma/\delta V_g$ in Figure 1e as $\mu = C^{-1}\delta\sigma/\delta V_g$. Here, C is the device channel-to-gate capacitance $C = \epsilon\epsilon_0/d$, where d is the dielectric thickness. The capacitance was determined independently using Hall measurements. The field-

effect mobilities plotted vs temperature (see Figure 1e inset) are nearly constant below 80 K, decreasing as $T^{-\alpha}$ above 100 K with α varying from 0.6 to 1.5 depending on the carrier type and crystallographic direction. We interpret the $T^{-\alpha}$ as the onset of electron−phonon scattering.

At low temperatures (5−50K) the hole mobility values were approximately 1500 and 500 cm^2 V^{-1} s^{-1} for transport along the x and y axes, respectively. The corresponding electron mobility values were somewhat smaller, approximately 1200 and 200 cm^2 V^{-1} s^{-1}, respectively. The anisotropy of mobility was, therefore, between 2 and 4. Accounting for the Drude relation between mobility and conductivity, $\sigma = ne\mu$, yields the ratio $A = \sigma_{xx}/\sigma_{yy}$ as 1.5 $\pm$ 0.1 and 2.6 $\pm$ 0.1 for devices A and B, respectively (see Figure 2c). Such a large spread in the apparent
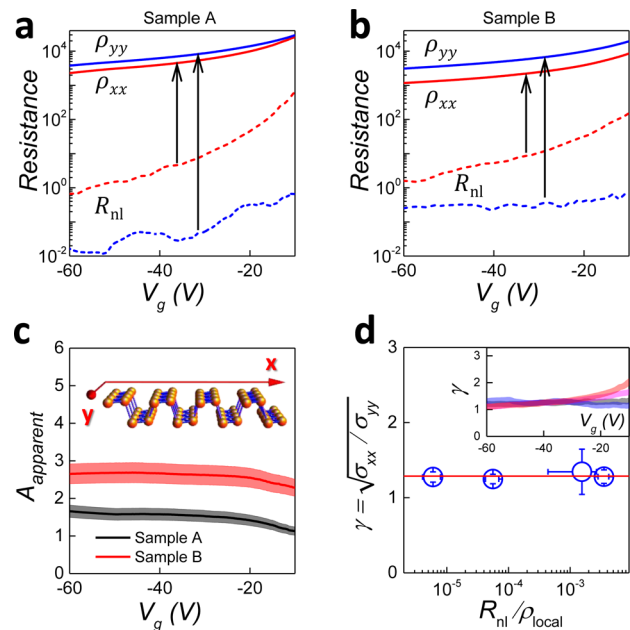

Figure 2. Transport anisotropy of black phosphorus devices, T = 5 K. (a), (b) Resistance vs gate voltage measured for samples A and B along principal crystallographic axes (red, x axis; blue, y axis; see panel c inset). Solid lines: local resistivity ρ_{xx} and ρ_{yy}. Dashed lines: nonlocal resistance R_{nl}. Noise level $\approx$ 0.05 Ω. (c) Apparent anisotropy $A_{apparent}$ = σ_{xx}/σ_{yy} measured as the ratio of the local (longitudinal) conductivities of the Hall bars aligned with the x and y axes. (d) Anisotropy coefficient (averaged for V_g varying from −20 V to −60 V) determined from the ratio of the nonlocal to local resistance, using $\rho_{local} = \rho_{xx}$ for $R_{nl}^{(x)}$ and $\rho_{local} = \rho_{yy}$ for $R_{nl}^{(y)}$. Inset shows the anisotropy coefficient vs gate voltage for both samples and both crystallographic axes (Sample A: x axis, red; y axis, blue. Sample B: x axis, magenta; y axis, black).

anisotropy values illustrates the pitfalls of this direct approach for accurate determination of anisotropy, eq 1. The large spread arises even when the different devices used are made from the same crystal, and with a well-defined Hall bar geometry.

One can identify two main reasons for the direct method to lack precision.[11] First, the value A is obtained from conductivity measurements on physically different samples with somewhat different conductivity tensors. Second, even for well-defined geometry the aspect ratio might vary slightly from sample to sample. With our new method, on the other hand, both local and nonlocal measurements are done on the same device; thus, we eliminate these two sources of inaccuracy. Further, the exponential sensitivity of the nonlocal response to the anisotropy value gives the nonlocal method a distinct advantage

over local measurements in finding the true conductance anisotropy.

Next, we proceed to discuss the nonlocal resistance measurements. Due to the high contact resistance, which is at least an order of magnitude larger than the channel resistance, we are able to reliably assess nonlocal resistances only in a region of V_g from -10 V to -60 V, where the contact resistance is relatively small. We obtain nonlocal resistance by passing the current transverse the device channel (e.g., from contact 2 to 3 in Figure 1b) and by measuring a voltage drop across the nearest pair of potential contacts (e.g., between contacts 4 and 5 in Figure 1b). Figure 2a and b summarize results of our measurements for both local and nonlocal resistances using the two studied devices and both principal crystallographic axes. Nonlocal resistance was several orders of magnitude lower than the local resistance and was also considerably lower along the y axis than along the x axis. Comparing panels a and b in Figure 2, the difference in the nonlocal resistance values measured along the x and y axes is larger for the device with $L/W = 3$ than for the one with $L/W = 2.5$.

This behavior can be exemplified by four-terminal measurements in device B (in our discussion below, we refer to the schematics shown in Figure 1a,b). Nonlocal resistance measured along the x axis, $R_{nl} = V_{4,5}/I_{2,3}$, is a factor of 5–20 larger than the one measured along the y axis, $R_{nl} = V_{9,10}/I_{7,8}$, see dashed red and blue lines in Figure 2b. Indeed, as discussed above, because current between contacts 2 and 3 flows along the hard (low-conductivity) direction, it tends to spread along the Hall bar channel (x axis), resulting in a larger voltage drop across contacts 4 and 5. In contrast, current between contacts 7 and 8 flows along the easy (high-conductivity) direction and, therefore, is pinched into a relatively narrow channel and spreads much less in the hard direction along the Hall bar channel (y axis). This results in a much smaller voltage drop at remote contacts 9 and 10.

As discussed above, an anisotropic conductor can be treated as an isotropic one after an appropriate coordinate transformation.[9] This is accomplished by stretching/shrinking the device dimensions by a factor of $\gamma = \sqrt{\sigma_{xx}/\sigma_{yy}}$ and replacing the anisotropic conductivity tensor by an "average conductivity value", eq 4, giving

$$R_{nl}^{(x)} = \frac{4\gamma\rho_{xx}}{\pi}\exp\left(-\frac{\pi L}{W\gamma}\right), \qquad R_{nl}^{(y)} = \frac{4\rho_{yy}}{\pi\gamma}\exp\left(-\frac{\pi L\gamma}{W}\right) \tag{7}$$

respectively. Hence, for a fixed geometry, the ratio of the nonlocal and local resistance depends only on the anisotropy coefficient γ. This enables us to extract γ directly by combining the local and nonlocal measurements on a single Hall bar. Notably, Figure 2d inset shows that γ values are very similar for both devices and both crystallographic orientations of the Hall bars and is almost independent of gate voltage. Small deviations in γ for $V_g > -20$ V stem from complications of current pathways as the Fermi level approaches band gap. Figure 2d summarizes data from Figure 2a and b and demonstrates the close agreement of anisotropy coefficient for both studied devices yielding $\gamma \equiv \sqrt{\sigma_{xx}/\sigma_{yy}} \approx 1.29 \pm 0.05$ and, hence, the anisotropy value $A \equiv \sigma_{xx}/\sigma_{yy} \approx 1.66 \pm 0.1$.

It is interesting to compare these results with the anisotropy in bulk BP. Anisotropy of Hall mobility measured at about 50 K for p-type crystals was about 3.3 (ref 23), which is notably

larger than the values found in our experiment as well as the values reported in refs 6 and 7. The twice smaller anisotropy of in-plane conductance of a few-layer phosphorene as compared to the bulk BP can be attributed to the surface scattering, which reduces the anisotropy of electron–phonon interaction.[24] The anisotropic electron–phonon interactions as well as the anisotropic properties of acoustic phonons in black phosphorus could also lead to the anisotropy in Drude relaxation times τ_{yy}/τ_{xx}.[25] The latter could explain the difference between the anisotropies of conductance and effective mass in BP. From previous measurements[26] and theory[27,28] the ratio of effective masses along the x and y directions $m_{eff}^{yy}/m_{eff}^{xx}$ was estimated at 7.7 ± 1.2, which is much larger than the conductance anisotropy measured in this work. At constant carrier concentrations, the difference of the two anisotropies could be accounted for by the anisotropy $\tau_{yy}/\tau_{xx} \approx 4.4 \pm 1.1$. It would be interesting to find out how these anisotropies evolve with decreasing the number of layers down to monolayer phosphorene, but unfortunately, such encapsulated BP devices will require remote-controlled microfabrication in an inert atmosphere,[17] which at present appears to be very challenging.

Lastly, we note that the nonlocal resistance observed in BP has a purely classical explanation, thus differing from nonlocal responses observed in systems with nontrivial band properties due to either spin–orbit coupling (spin Hall effect) or nonzero Berry curvature (anomalous/valley Hall effect). In these two cases, the nonlocal resistance is a manifestation of a combination of direct and inverse spin/anomalous Hall effects, induced by the presence of spin- or valley-polarized currents. These effects should play only a minor role (if any) in the nonlocal transport in BP because phosphorus is a light element and the spin–orbit terms do not contribute appreciably to BP band structure.[28] Moreover, topology of a band structure near the Γ point of BP Brillouin zone is trivial (single valley),[29] leading to zero Berry curvature and, thus, to the absence of topological currents.[30]

Summing up, we have described a new approach to characterize transport anisotropy of layered nanomaterials, which has distinct advantages over previously developed approaches. Our method leverages on novel measurement schemes (nonlocal response) through which the effect of anisotropy can be sharply enhanced and accessed directly without resorting to traditional angle-resolved approaches. Namely, our method utilizes the combination of local and nonlocal transport measurements and relies on the exponential sensitivity of nonlocal resistance to the anisotropy coefficient. Using this method, we find that the anisotropy of in-plane conductance σ_{xx}/σ_{yy} for thin BP crystals amounts to $\approx 1.66 \pm 0.1$. This method can easily be adapted to other anisotropic 2D crystals (e.g., ReSe$_2$ and ReS$_2$) as well as for 2D materials and heterostructures where in-plane anisotropy might be induced via strain or charge density waves.

■ ASSOCIATED CONTENT

⑤ Supporting Information

The Supporting Information is available free of charge on the ACS Publications website at DOI: 10.1021/acs.nano-lett.5b03004.

Proof of the anamorphosis theorem and direct derivation of the nonlocal response for a strip geometry. (PDF)

■ AUTHOR INFORMATION

Corresponding Authors
*E-mail: artem.mishchenko@gmail.com.
*E-mail: levitov@mit.edu.

Author Contributions
A.M., Y.C., and G.L.Y. contributed equally.

Notes
The authors declare no competing financial interest.

■ REFERENCES

(1) Brown, A.; Rundqvist, S. Refinement of the crystal structure of black phosphorus. *Acta Crystallogr.* **1965**, *19*, 684−685.

(2) Takao, Y.; Asahina, H.; Morita, A. Electronic Structure of Black Phosphorus in Tight Binding Approach. *J. Phys. Soc. Jpn.* **1981**, *50*, 3362−3369.

(3) Ling, X.; Wang, H.; Huang, S.; Xia, F.; Dresselhaus, M. S. The renaissance of black phosphorus. *Proc. Natl. Acad. Sci. U. S. A.* **2015**, *112*, 4523−4530.

(4) Fei, R.; Faghaninia, A.; Soklaski, R.; Yan, J.-A.; Lo, C.; Yang, L. Enhanced Thermoelectric Efficiency via Orthogonal Electrical and Thermal Conductances in Phosphorene. *Nano Lett.* **2014**, *14*, 6393−6399.

(5) Low, T.; Roldán, R.; Wang, H.; Xia, F.; Avouris, P.; Moreno, L. M.; Guinea, F. Plasmons and Screening in Monolayer and Multilayer Black Phosphorus. *Phys. Rev. Lett.* **2014**, *113*, 106802.

(6) Xia, F.; Wang, H.; Jia, Y. Rediscovering black phosphorus as an anisotropic layered material for optoelectronics and electronics. *Nat. Commun.* **2014**, *5*, 4458.

(7) Liu, H.; Neal, A. T.; Zhu, Z.; Luo, Z.; Xu, X.; Tománek, D.; Ye, P. D. Phosphorene: an unexplored 2D semiconductor with a high hole mobility. *ACS Nano* **2014**, *8*, 4033−4041.

(8) van der Pauw, L. J. A method of measuring the resistivity and hall coefficient on lamellae of arbitrary shape. *Philips Technical Review* **1958**, *20*, 220−224.

(9) See Supporting Information.

(10) Price, W. L. V. Extension of van der Pauw's theorem for measuring specific resistivity in discs of arbitrary shape to anisotropic media. *J. Phys. D: Appl. Phys.* **1972**, *5*, 1127−1132.

(11) Simon, S. H. Comment on Evidence for an Anisotropic State of Two-Dimensional Electrons in High Landau Levels. *Phys. Rev. Lett.* **1999**, *83*, 4223−4223.

(12) Bierwagen, O.; Pomraenke, R.; Eilers, S.; Masselink, W. Mobility and carrier density in materials with anisotropic conductivity revealed by van der Pauw measurements. *Phys. Rev. B: Condens. Matter Mater. Phys.* **2004**, *70*, 165307.

(13) Mele, E. J. Screening of a point charge by an anisotropic medium: Anamorphoses in the method of images. *Am. J. Phys.* **2001**, *69*, 557.

(14) Wait, J. R. Current flow into a three-dimensionally anisotropic conductor. *Radio Sci.* **1990**, *25*, 689−694.

(15) Abanin, D. A.; Morozov, S. V.; Ponomarenko, L. A.; Gorbachev, R. V.; Mayorov, A. S.; Katsnelson, M. I.; Watanabe, K.; Taniguchi, T.; Novoselov, K. S.; Levitov, L. S.; et al. Giant nonlocality near the Dirac point in graphene. *Science (Washington, DC, U. S.)* **2011**, *332*, 328−330.

(16) Island, J. O.; Steele, G. A.; van der Zant, H. S. J.; Castellanos-Gomez, A. Environmental instability of few-layer black phosphorus. *2D Mater.* **2015**, *2*, 011002.

(17) Cao, Y.; Mishchenko, A.; Yu, G. L.; Khestanova, E.; Rooney, A. P.; Prestat, E.; Kretinin, A. V.; Blake, P.; Shalom, M. B.; Woods, C.; et al. Quality Heterostructures from Two-Dimensional Crystals Unstable in Air by Their Assembly in Inert Atmosphere. *Nano Lett.* **2015**, *15*, 4914−4921.

(18) Wang, L.; Meric, I.; Huang, P. Y.; Gao, Q.; Gao, Y.; Tran, H.; Taniguchi, T.; Watanabe, K.; Campos, L. M.; Muller, D. A.; et al. One-dimensional electrical contact to a two-dimensional material. *Science* **2013**, *342*, 614−617.

(19) Kretinin, A. V.; Cao, Y.; Tu, J. S.; Yu, G. L.; Jalil, R.; Novoselov, K. S.; Haigh, S. J.; Gholinia, A.; Mishchenko, A.; Lozada, M.; et al. Electronic properties of graphene encapsulated with different two-dimensional atomic crystals. *Nano Lett.* **2014**, *14*, 3270−3276.

(20) Zhang, S.; Yang, J.; Xu, R.; Wang, F.; Li, W.; Ghufran, M.; Zhang, Y.-W.; Yu, Z.; Zhang, G.; Qin, Q.; et al. Extraordinary photoluminescence and strong temperature/angle-dependent Raman responses in few-layer phosphorene. *ACS Nano* **2014**, *8*, 9590−9596.

(21) Britnell, L.; Gorbachev, R. V.; Jalil, R.; Belle, B. D.; Schedin, F.; Katsnelson, M. I.; Eaves, L.; Morozov, S. V.; Mayorov, A. S.; Peres, N. M. R.; et al. Electron tunneling through ultrathin boron nitride crystalline barriers. *Nano Lett.* **2012**, *12*, 1707−1710.

(22) Li, L.; Yu, Y.; Ye, G. J.; Ge, Q.; Ou, X.; Wu, H.; Feng, D.; Chen, X. H.; Zhang, Y. Black phosphorus field-effect transistors. *Nat. Nanotechnol.* **2014**, *9*, 372−377.

(23) Akahama, Y.; Endo, S.; Narita, S.-I. Electrical Properties of Black Phosphorus Single Crystals. *J. Phys. Soc. Jpn.* **1983**, *52*, 2148−2155.

(24) Luo, Z.; Maassen, J.; Deng, Y.; Du, Y.; Lundstrom, M. S.; Ye, P. D.; Xu, X. Anisotropic in-plane thermal conductivity observed in few-layer black phosphorus. 2015, arXiv:1503.06167. arXiv.org e-Print archive. http://arxiv.org/abs/1503.06167 (accessed September 2015).

(25) Morita, A.; Sasaki, T. Electron-Phonon Interaction and Anisotropic Mobility in Black Phosphorus. *J. Phys. Soc. Jpn.* **1989**, *58*, 1694−1704.

(26) Narita, S.-I.; Terada, S.-i.; Mori, S.; Muro, K.; Akahama, Y.; Endo, S. Far-Infrared Cyclotron Resonance Absorptions in Black Phosphorus Single Crystals. *J. Phys. Soc. Jpn.* **1983**, *52*, 3544−3553.

(27) Morita, A. Semiconducting black phosphorus. *Appl. Phys. A: Solids Surf.* **1986**, *39*, 227−242.

(28) Qiao, J.; Kong, X.; Hu, Z.-X.; Yang, F.; Ji, W. High-mobility transport anisotropy and linear dichroism in few-layer black phosphorus. *Nat. Commun.* **2014**, *5*, 4475.

(29) Rudenko, A. N.; Katsnelson, M. I. Quasiparticle band structure and tight-binding model for single- and bilayer black phosphorus. *Phys. Rev. B: Condens. Matter Mater. Phys.* **2014**, *89*, 201408.

(30) Lensky, Y. D.; Song, J. C. W.; Samutpraphoot, P.; Levitov, L. S. Topological Valley Currents in Gapped Dirac Materials. *Phys. Rev. Lett.* **2015**, *114*, 256601.